Validation of Mass-Transfer Model for VIPS Process using In Situ Measurements Performed by Near-Infrared Spectroscopy

D. Bouyer and C. Pochat-Bohatier
UMR 5635 - CNRS, ENSCM, UM II, Institut Européen des Membranes, place Eugène Bataillon, 34095 Montpellier, Cedex 5, France

DOI 10.1002/aic.13839
Published online June 20, 2012 in Wiley Online Library (wileyonlinelibrary.com).

Combined experimental and modeling approaches were performed in order to investigate the influence of formulation and process parameters on mass transfers during VIPS process, using the water/N-methyl-pyrrolidone (NMP)/poly(ether imide) (PEI) system. The experiments were conducted using a thick polymer solution at increasing polymer concentrations for various operating conditions. The global water intake rate in the bulk solution was determined by gravimetric measurements (global), and in situ *measurements were conducted by near-infrared spectroscopy at three points in the solution. In parallel, a fully predictive model was developed for predicting mass-transfer phenomena involved during the VIPS process. The comparison between experimental data and numerical predictions exhibited a good agreement for moderate polymer concentration, but for higher polymer concentrations, the model overestimated the nonsolvent-transfer rate. This result was explained by the aggregation process of the polymer chains due to water intake. The numerical predictions were improved by modifying the average hole-free volume expression.* © 2012 American Institute of Chemical Engineers *AIChE J,* 59: 671–686, 2013
Keywords: membrane elaboration, VIPS process, mass-transfer modeling

Introduction

Phase separation process background

The phase separation process is widely used for producing porous polymeric membranes, whose morphology depend on multiple factors such as polymer concentration, solvent quality or the phase inversion process involved. The demixion of the polymeric system can be induced by a temperature change, usually a temperature decrease, i.e., temperature induced phase separation (TIPS), above the upper critical solution temperature (UCST), and by solvent evaporation (dry cast), or nonsolvent induced phase separation (NIPS). The NIPS process consists in inducing the demixion by nonsolvent intake into a binary polymer/solvent solution, and it involves (1) the vapor induced phase separation (VIPS) process that consists in transferring the nonsolvent from the gas phase, and (2) the immersion (or wet casting) process, which consists in placing the polymer solution into a nonsolvent bath.[1–5] The wet casting process involves rapid mass-transfer rates (solvent extraction and nonsolvent penetration), and usually leads to asymmetric membranes characterized by macrovoids structures. Such membranes are characterized by high-permeation fluxes due to their large porosity. On the contrary, using the VIPS process, the mass-transfer rates are strongly reduced since the driving force is controlled by the volatility of the transferring components. In that respect, water is usually used as the nonsolvent such as its concentration in the gaseous phase can be easily controlled by the relative humidity (RH) and temperature.[6–10] Symmetric or asymmetric membranes can be fabricated by this process depending on both the polymeric system and process parameters.

Numerical model

Mathematical models have been recently developed for better description, understanding and predicting membrane formation mechanisms. All phase inversion processes have been simulated using numerical models, which continuously integrate greater complexity in order to take into account the whole transfer mechanisms. Most of them are valid until the demixion, i.e., until polymer-rich and polymer-lean phases separate; moreover, they usually include a mathematical description of thermodynamics and multicomponent mass transfers, sometimes coupled to heat transfers.

Numerical models were developed later for the VIPS process, since there has been an increasing interest for this process in the last decade. The first mass-transfer model included single-diffusion coefficients determined by the free-volume theory rather than cross-diffusion coefficients.[6] More recently, more sophisticated models have been proposed, which aimed at testing the influence of process parameters on membrane morphologies.[11–12] Their numerical predictions have been compared to experimental studies reported in the literature. Yip and McHugh[12] have incorporated coupled mass and heat transfer, ternary diffusion and moving boundary at the interface. They incorporated a diffusion model derived from the friction-based diffusion model proposed by Alsoy and Duda[13] and tested different systems, such as

Correspondence concerning this article should be addressed to D. Bouyer at denis.bouyer@um2.fr.

cellulose acetate/acetone/water, poly(vinylidene fluoride) (PVDF)/dimethylformamide (DMF)/water, polysulfone (PS)/N-methyl-2-pyrolidone (NMP)/water, and poly(ether imide) (PEI)/NMP/water. Khare et al.[11] proposed a mathematical model that was similar to the model for evaporative-casting developed by Shojaie et al.[14] They studied the quaternary water/N-methyl-pyrrolidone (NMP)/poly(ether sulfone) (PES)/polyvinyl pyrrolidone (PVP) system, and aimed at predicting the morphology of the final membranes especially in the case of forced airflow conditions. Their model incorporated transport mechanisms directly derived from Bearman's relationship between the thermodynamic driving forces and the mass fluxes.[15] The influence of the diffusion formalism on the concentration profiles were also tested using the poly(ether imide) (PEI)/NMP/water system.[16] The choice of the operating parameters (process parameters and polymer concentration) was discussed in terms of final membrane morphology.

Experimental validation

Although several numerical models have been developed, their validation using experimental results is still tricky. A complete model that aims at being fully predictive integrates lots of independent parameters in the diffusion equations or in the empirical correlations, which should be determined using independent experiments. Consequently, the numerical results given by the model depend on various parameters; therefore, its validation is quite difficult and requires dedicated and localized experiments. However, the most common experimental validation reported in the literature is the gravimetric measurements, i.e., the variation of the global casting film weight during the process.[6,14,17] Also, for numerical models that incorporated coupled mass and heat transfer, the variation of the interface temperature have been followed and compared to simulated predictions. For other models, the numerical results have been directly compared to morphological properties of the membranes. In that case, the concentration profiles along the casting film thickness have been compared to the spatial distribution of the pore size.[11,16,18] More recently, an isothermal mass-transfer model was developed for TIPS process including the polymer crystallization kinetics.[19] They compared their results to the spherulite diameter obtained at different cooling rates. Previously, observations on the dynamics of NIPS have been performed to validate a diffusion model, using a diffusion cell and a video imaging technique. In this case, both the diffusion front motion and the morphologies have been followed for various quench compositions.[20–21] Nevertheless, to the best of our knowledge, the numerical models concerning phase inversion processes have never been validated using direct concentration profiles within the polymer solution. The main concern is the difficulty in measuring the solution composition during the process using *in situ* and *in line* measurements. However, recently, a methodology was proposed in order to follow the variation of the concentration profiles during VIPS process in deeper polymer solution using near-infrared spectroscopy (NIRS).[22]

Scope of this article

In this study, the modeling approach of the VIPS process was not only validated by global data such as gravimetric measurement, but also by *in situ* local experiments conducted during the process. The solution composition was followed at three points at increasing depth beneath the air/solution interface by NIRS, which allowed determining the nonsolvent-transfer rate and the concentration profiles. Such local measurements were also used to validate the mass- and heat-transfer model in various operating conditions and for increasing polymer concentrations. Two conditions of temperature were tested (40 and 25°C) under different conditions of relative humidity (43 and 75%), and quiescent hydrodynamic conditions in the VIPS chamber.

The mathematical model is developed in the first part of this article, and the equations needed to simulate the mass-transfer phenomena will be detailed. The experimental results obtained by NIRS will then be presented, focusing on the water intake rate during the process under various operating conditions. Such experimental data will then be compared to numerical prediction to discuss the model reliability. Slight modification of the diffusion model will also be made for the highest polymer concentration to improve the agreement between numerical predictions and experimental data.

Materials and Methods

Preparation of polymer solutions

PEI (poly(bisphenol A-*co*-4-nitrophtalic anhydride-*co*-1,3-phenylenediamine)) from Aldrich, was dried for 24 h at 170°C *in vacuo* before use. Anhydrous NMP was purchased from Aldrich and used without any further purification. The polymer solutions (12, 16, and 20 wt. %) were prepared at room temperature by stirring PEI in NMP for 5 days in a glovebox, where the relative humidity was kept below 7% and processed within a week after being prepared.

Design of the experimental procedure

The PEI solution was first introduced into a 10 mm spectroscopy rectangular cell in quartz suprasil® with PTFE lid. The depth of the polymer solution was 18 mm. The surface/volume ratio was calculated to be ca 0.6 cm^{-1}. The open cell was then placed in a closed vessel at 40 $\pm$ 1°C, with an atmosphere controlled by a saturated salt solution (NaCl for 75% RH). Experiments were carried out in static mode, i.e., without any air circulation. The cell was repetitively taken out the vessel at regular times, and closed with the PTFE lid to prevent atmospheric water vapor absorption. The weight increase of the polymer solution was determined by gravimetric measurement (Precisa XT 120A, Precisa Instrument, Ltd., Switzerland). At the same time near-infrared spectroscopy analyses were performed. All these operations were conducted as quickly as possible so as not to disturb the water absorption experiments.

Near-infrared spectroscopy (NIRS)

NIRS Measurements. Fourier transform NIRS in transmission mode was used to determine the water mass fraction of the polymeric solution. NIR spectra were recorded every 30 min using a PerkinElmer Spectrum One NTS equipped with a tungsten-halogen lamp, a quartz envelope as the light source, and also a deuterated triglycine sulfate (DTGS) detector. The instrument was driven by the Spectrum v3.02 software from PerkinElmer for data scanning and processing. The function "atmospheric suppression" of the instrument was activated in the absorption bands to remove the contribution of the atmospheric CO_2 and water vapor.

Four scans were averaged at a 4 cm^{-1} resolution in the range of 2,600–10,000 cm^{-1}. The size of the NIR spot was

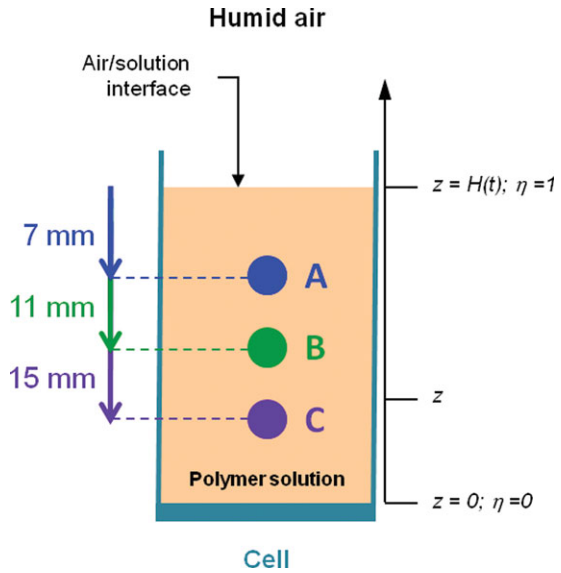

Figure 1. Schematic of VIPS process performed in the deep cell dedicated to NIRS.

[Color figure can be viewed in the online issue, which is available at wileyonlinelibrary.com.]

set equal to 2.5 mm dia., and the analyses were performed at increasing depths within the polymer solution: 7 mm (point A), 11 mm (point B), and 15 mm (point C), under the air/solution interface (Figure 1).

Data processing

Quantitative analyses were achieved on the obtained spectra with a multivariate calibration model to determine the water mass fraction. A set of 43 standard ternary solutions with a well-defined composition of PEI (from 0 to 27 wt. %), NMP (from 70 to 100 wt. %), and water (from 0 to 6 wt. %), were prepared and spectra were obtained for each sample. This collection of spectra was used to build the calibration model, using the statistical Spectrum Quant^{+} v4.51 software from PerkinElmer, and based on partial least-squares (PLS) data treatment. The transmission spectra were processed in the range of 7,500– 5,800 cm^{-1}, because the absorption bands at 7,000, 6,900, and 6,450 cm^{-1} were attributed to water. The maxima located at 6,900 cm^{-1} was assigned to the first overtone of the OH-stretching band (2 $\nu_{1,3}$) of the water molecule.

The calibration model was then validated by full cross-validation. The standard error of calibration (SEC), the standard error of cross-validation (SECV), and the correlation coefficient (R^2) were, respectively, 0.0.044, 0.049, and 99.92% for water prediction. The whole procedure was fully explained in a previous article[22] and gives accurate results for water mass fraction monitoring during exposure of polymer solution to air.

Model Description

The phase inversion induced by VIPS process is governed by solvent and nonsolvent fluxes perpendicular to the polymer solution. Initially, the binary polymer solution is assumed to have uniform composition. Once the polymer solution is exposed to humid air, the nonsolvent (water) takes in the solution, whereas the solvent evaporates. Cross diffusions are also involved within the solution. The mass-transfer model presented in this article has been presented elsewhere,[16] with the main equations remaining. It involves a coupling between mass and heat transfer; the diffusion formalism is based on the friction-based diffusion model, and self-diffusion coefficients were calculated using the free-volume theory developed by Vrentas and Duda,[23–24] and extended by Alsoy and Duda[13] for multicomponent diffusion systems.

Description of the geometry

The geometry for mass and heat transfer in this system is presented in Figure 1. The polymer solution is placed in a deep cell and exposed to humid air. The mass transfer is assumed to be one-dimensional (1-D) in the vertical axis. Since the thickness of the polymer solution considered in this work is high compared to thin membranes, the heat-transfer equation must be solved within the domain, meaning that the lumped parameter approach is not sufficient. The gas phase next to the topside of the polymer solution is characterized by temperature T^g, the relative humidity HR, and the partial pressure of each volatile compound.

Thermodynamics

A thermodynamic model is necessary for two main reasons: (1) the multicomponent mass transfer involves the local chemical potential gradients, which can be calculated once the ternary interaction parameters are known, and (2) the mass exchanges between the air and solution are controlled by the activity difference of all transferring species. According to Flory-Huggins theory, the Gibbs free-energy-of-mixing in a ternary system is given by the following relation

$$\frac{\Delta G_m}{RT} = \sum_{i=1}^{3} n_i ln\phi_i + g_{12} n_1 \phi_2 + \chi_{13} n_1 \phi_3 + \chi_{23} n_2 \phi_3 \qquad (1)$$

where n_i and ϕ_i are the number of moles and volume fraction of component i, R and T are the universal constant and temperature, respectively. g_{12}, χ_{13} and χ_{23} are the solvent/nonsolvent, nonsolvent/polymer and solvent/polymer interaction parameters, respectively. The value of g_{12} depends on the ratio between the solvent and nonsolvent.[25] The chemical potential of each component was calculated from the derivation of the Gibbs free energy by the molar number n_i.[16]

Mass-transfer model

As mentioned earlier, only the main equations will be used in this article, and the equation that differs from a previously published model.[16] The 1-D mass-transfer model integrates the following assumptions: (1) it was assumed that the polymer did not transfer to the air side; (2) ideal gas behavior was considered at the air side, and (3) gas-liquid equilibrium was assumed at the air/solution interface. Moreover, the excess of volume due to mixing was neglected. Based on these assumptions and a coordinate transform (η = z/H), the mass-transfer model equations were derived as follows

$$\frac{\partial \rho_i}{\partial t} = \frac{\eta}{H(t)} \frac{\partial H(t)}{\partial t} \frac{\partial \rho_i}{\partial \eta} + \frac{1}{H(t)^2} \frac{\partial}{\partial \eta} \left(- \sum_{j=1}^{2} D_{ij} \frac{\partial \rho_j}{d\eta} \right) \quad i = 1, 2 \qquad (2)$$

In previous studies, the heat transfer has been simulated using a lumped parameter approach,[12,16] assuming uniform temperature in the casting film. In this case, since the thickness of the solution placed in the cell is much higher (18

Table 1. Free Volume and Flory-Huggins Interaction Parameters used in the Simulations

Parameter	Unit	Value	Reference
V_1*	cm^3/g	1.071	Yip and McHugh (2006)
V_2*	cm^3/g	0.841	Yip and McHugh (2006)
V_3*	cm^3/g	0.663	Yip and McHugh (2006)
K_{11}/γ	$cm^3/(g.K)$	0.00218	Yip and McHugh (2006)
K_{12}/γ	$cm^3/(g.K)$	0.000963	Yip and McHugh (2006)
K_{13}/γ	$cm^3/(g.K)$	0.000452	Yip and McHugh (2006)
K_{21}-T_{g1}	K	−152.29	Yip and McHugh (2006)
K_{22}-T_{g2}	K	−48.496	Yip and McHugh (2006)
K_{23}-T_{g3}	K	−443	Yip and McHugh (2006)
D_{01}	cm^2/s	$8.55\ 10^{-4}$	Yip and McHugh (2006)
D_{02}	cm^2/s	$3.14\ 10^{-4}$	Yip and McHugh (2006)
χ_{13}	-	2.1	Yip and McHugh (2006)
χ_{23}	-	0.507	Yip and McHugh (2006)
ζ_{13}	-	0.0909	Yip and McHugh (2006)
ζ_{23}	-	0.393	Yip and McHugh (2006)
a_0	-	0.5483	Wei *et al.* (2006)
a_1	-	−0.092	Wei *et al.* (2006)
a_2	-	2.0522	Wei *et al.* (2006)
a_3	-	−3.9428	Wei *et al.* (2006)
a_4	-	2.6792	Wei *et al.* (2006)

mm), the lumped parameter approach is not relevant and the heat-transfer equation must be solved within the solution. The heat equation is written as follows

$$\frac{\partial T}{\partial t} = \frac{\alpha}{H(t)^2}\frac{\partial^2 T}{\partial \eta^2} \tag{3}$$

where α represents the thermal diffusivity of the polymer solution ($\alpha = k_p/(\rho_p C_{pp})$), with k the thermal conductivity of the polymer solution, ρ its density, and C_p its heat capacity. Because of the low thickness of the glass plate compared to the polymer solution thickness, the heat-transfer resistance was neglected in the glass plate.

Initial and boundary conditions

Initially, the solution is nonsolvent free (null concentration), and the solvent concentration is ranged between 80 and 88%, depending on the polymer concentration. The solvent concentration is uniform in the polymer solution at initial time. Moreover, the initial temperature is equal to 20°C.

Concerning the boundary conditions, symmetry conditions were assumed for mass transfer at the substrate/solution interface, but flux conditions were assumed at the air/solution interface. Dirichlet boundary conditions for heat transfer are fixed at $\eta = 0$, since the sample is placed onto a glass plate in direct contact with the bottom of the heater, which is in equilibrium with the VIPS chamber temperature (T^g).

$\eta = 0$

$$-\frac{\partial \rho_1}{\partial \eta} = -\frac{\partial \rho_2}{\partial \eta} = 0 \tag{4}$$

$$T = T^g \tag{5}$$

At $\eta = 1$, Neumann conditions are simulated

$$\left(-\frac{D_{11}}{H(t)}\frac{\partial \rho_1}{\partial \eta} - \frac{D_{12}}{H(t)}\frac{\partial \rho_2}{\partial \eta}\right) - \rho_1\frac{dH(t)}{dt} = J_1^g = k_1\left[\rho_{1g}^i(T^i) - \rho_{1g}^\infty(T^g)\right] \tag{6}$$

$$\left(-\frac{D_{21}}{H(t)}\frac{\partial \rho_1}{\partial \eta} - \frac{D_{22}}{H(t)}\frac{\partial \rho_2}{\partial \eta}\right) - \rho_2\frac{dH(t)}{dt} = J_2^g = k_2\left[\rho_{2g}^i(T^i) - \rho_{2g}^\infty(T^g)\right] \tag{7}$$

$$\frac{\lambda}{H(t)}\frac{\partial T}{\partial \eta} - \rho C_p T\frac{dH(t)}{dt} = h\left(T^i - T^g\right) + \sum_{i=1}^{2} J_i^g \Delta H v_i \tag{8}$$

where ρ_{ig}^i and ρ_{ig}^∞ are the concentrations of component i at the air/solution interface and in the gas phase, respectively. At the interface, the concentrations were estimated from the activity, which derived from the chemical potential, and, thus, from the Gibbs free energy given by Flory-Huggins theory.[16] The gas phase was considered as an infinite volume, therefore, the solvent concentration was assumed to be null. Assuming that water vapor is an ideal gas, its concentration in the gas phase could be estimated. ΔHv_1 and ΔHv_2 are the enthalpy of vaporization for nonsolvent and solvent, respectively. k_1 and k_2 are the mass-transfer coefficients of nonsolvent and solvent.

A global mass balance is used to follow the variation of the solution thickness during the process

$$-\frac{dH(t)}{dt} = \frac{\sum_{i=1}^{2} J_i^g}{\rho_p} \tag{9}$$

Diffusion formalism

The mutual diffusion coefficients were expressed from the friction-based diffusion model presented in a previous study.[13] The influence of the diffusion formalism on the simulated results has also been discussed,[16] demonstrating that the following formalism was the most relevant

$$D_{ik} = \left(1 - \rho_i \hat{V}_i\right)\rho_i D_i\left(\frac{1}{RT}\frac{\partial \mu_i}{\partial \rho_k}\right) - \sum_{\substack{j=1 \\ j\neq i}}^{2} \rho_j \hat{V}_j \rho_i D_j\left(\frac{1}{RT}\frac{\partial \mu_j}{\partial \rho_k}\right) \quad i,k = 1,2 \tag{10}$$

The self-diffusion coefficients were calculated using the free-volume theory of Vrentas and Duda[24]

$$D_1 = D_{01}\exp\left(-\frac{w_1\hat{V}_1^* + w_2\hat{V}_2^*(\zeta_{13}/\zeta_{23}) + w_3\hat{V}_3^*\zeta_{13}}{\hat{V}_{FH}/\gamma}\right) \tag{11}$$

$$D_2 = D_{02}\exp\left(-\frac{w_1\hat{V}_1^*(\zeta_{23}/\zeta_{13}) + w_2\hat{V}_2^* + w_3\hat{V}_3^*\zeta_{23}}{\hat{V}_{FH}/\gamma}\right) \tag{12}$$

$$\frac{\hat{V}_{FH}}{\gamma} = \frac{K_{11}}{\gamma}(K_{21} - T_{G1} + T)w_1 + \frac{K_{12}}{\gamma}(K_{22} - T_{G2} + T)w_2 + \frac{K_{13}}{\gamma}(K_{23} - T_{G3} + T)w_3 \tag{13}$$

Free-volume parameters for the PEI/NMP/water system have been given by Yip and McHugh[12] (Table 1).

Mass-transfer coefficients

Empirical correlations were used to estimate the external mass-transfer coefficients. Free convection was assumed, considering that the air motion was induced by a density change in the vicinity of the air/solution interface. Although

Table 2. Physical Properties of the Water (1), NMP (2), PEI (3) and Air

Parameter	Unit	Value
M_1	g/mol	18
M_2	g/mol	99
M_3	g/mol	24000
$\hat{V}_1$	m^3/kg	10^{-3}
$\hat{V}_2$	m^3/kg	$9.709\ 10^{-4}$
$\hat{V}_3$	m^3/kg	$7.874\ 10^{-4}$
Lc	m	10^{-2}
ΔH_{v1}	J/g	2256
ΔH_{v2}	J/g	533
λ_p	J/(s.m.K)	$2.0\ 10^{-1}$
C_{pp}	J/(g.K)	2.5
λ_p	J/(s.m.K)	$2.26\ 10^{-2}$
M_{air}	g/mol	28.96
T_0	K	293.15

different correlations have been reported in the literature,[6,12,14] the following expressions seem to be the most appropriate for horizontal cooled plates facing upward in the laminar regime[12,26]

$$\frac{k_i\ L_c\ y_{air,lm}}{D_{ig}} = 0.27(Gr\ Sc_i)^{0.25} \tag{14}$$

$$\frac{h\ L_c}{k_a} = 0.27(Gr\ \ \mathrm{Pr})^{0.25} \tag{15}$$

The Grashof number (Gr) expresses free convection due to density difference caused by (1) composition gradients, and/or (2) temperature gradients in the vicinity of the air/solution interface. The details of the calculation have been published in a previous article.[16] The physical parameters used in the model were reported in Table 2.

Results

Experimental kinetic curves

VIPS process was performed for the PEI/NMP/water system at different polymer concentrations and for various process conditions. Two conditions of relative humidity (75 and 43%) were tested to focus on the influence of the mass-transfer driving force on the water intake rate in the polymer solution. Most of experiments were conducted at 40°C, but one was performed at 25°C to focus on the temperature impact on the transfer rates. Three polymer concentrations were tested to investigate the link between the properties of the polymer solution and the transport phenomena. The whole operating conditions were summarized in Table 3.

For all experiments, the variation of the global mass of the polymer solution was followed during a period of time. It was demonstrated in previous study that this curve can represent the global water intake because of the low NMP volatility (106 Pa at 40°C and 34 Pa at 25°C).[22] In each graph in Figure 2, the time to reach the phase separation at the air/solution interface was reported by a thick gray line, and it corresponded to the total whiteness of the upper surface. The experimental data were collected at three different points in the cell to enable the quantification of local concentration gradients. The experimental data collected at 40°C were reported in Figure 2, and the kinetic curves collected at 25°C were reported in Figure 3. For the PEI/NMP/water system, the binodal curve is crossed when the water concentration exceeds around 5 wt. %.[12]

Before phase separation at the air/solution interface, the main conclusions about the experimental data can be summarized as follows:

- For given process conditions, i.e., various conditions of temperature and relative humidity, the variation of the water concentration at points A, B, and C exhibited that the water transport rate in the solution decreased with increasing polymer concentration. This result confirms that the molecular diffusion coefficient of small species (solvent and nonsolvent) within a polymer solution tended to decrease when increasing the polymer concentration, i.e., reducing the free volume between polymer chains.
- Higher the polymer concentration, lower the time to reach the phase separation at the air/solution interfaces (Table 4).
- Both results are linked and confirmed that the higher the polymer concentration, the higher the concentration gradients in the solution. For high-polymer concentrations, the transport rate within the solution was expected to decrease because of the free-volume reduction, whereas the global water intake was less affected. Therefore, the water mass fraction tended to increase more rapidly just beneath the air/solution interface, because the nonsolvent diffusion rate toward the bottom of the solution was lower than the global water intake. In such conditions, significant concentration gradients were created, as observed in Figure 2 for the highest relative humidity (75%) and temperature (40°C). Because of the water accumulation in the upper solution region at high-polymer concentrations, the composition path crossed the bimodal curve earlier; hence, the phase separation was reached sooner (Table 4).

In addition, the experimental results exhibited that the concentration gradients were lessened when reducing the temperature and/or the relative humidity. Indeed, working at low temperatures and/or under low-relative humidity led to decreasing the driving force for mass transfer, especially for the nonsolvent. Thus, it did increase the mass-transfer resistance in the gas phase, but in the same time, the mass-transfer resistance within the solution was almost unchanged. However, the concentration gradients beneath the air/solution interface were lessened compared to previous results obtained at higher temperature and relative humidity.

Once the phase separation was observed at the air/solution interface, the water intake rate significantly decreased whatever the initial polymer concentration, meaning that the mass-transfer resistance within the solution suddenly increased (Figure 2). Indeed, the demixion induced the formation of a two-phase region near the air/solution interface. After phase inversion started, the nonsolvent had, thus, to cross a biphasic region before entering in the polymer solution. Moreover, the thickness of this heterogeneous region

Table 3. Summary of Experimental Conditions

Relative Humidity	Temperature	Polymer concentration		
		12 wt%	16 wt%	20 wt%
75%	40 °C	X	X	X
	25 °C	X		
43%	40 °C	X	X	X

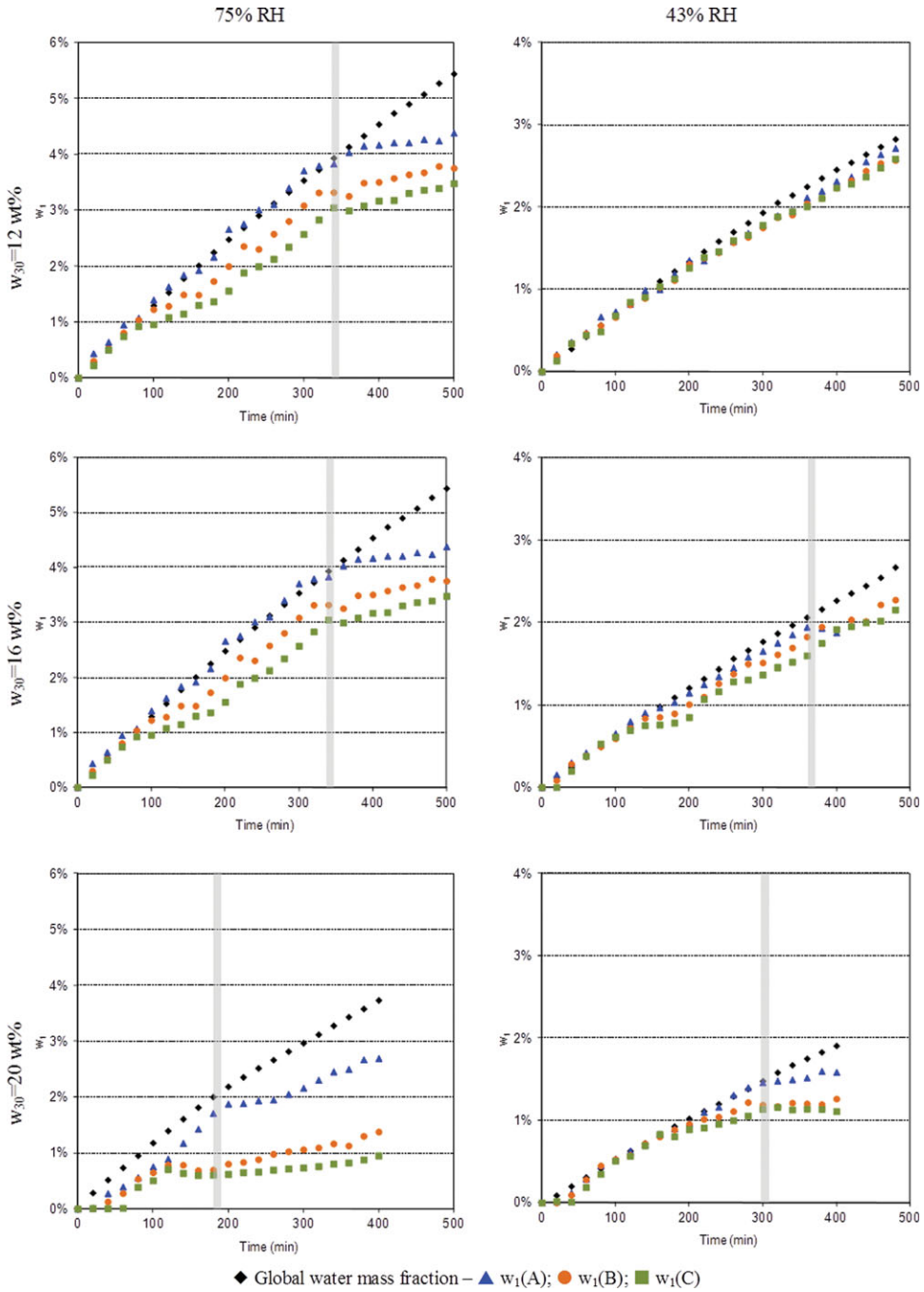

Figure 2. Variation as a function of time of the global water mass fraction and local water mass fractions at points A, B, and C: w_{30} = 12, 16 and 20 wt. %, T = 40°C, and RH = 75%.

[Color figure can be viewed in the online issue, which is available at wileyonlinelibrary.com.]

increased with time because of continuous water intake, leading to continuously enhance the internal mass-transfer resistance.

Furthermore, the global water mass fraction kept on increasing after phase separation, whereas a slop curve was observed on the local concentration curves (points A, B, and C). The difference between the global and the local water mass fractions increased with time, indicating that the water accumulated in the upper region of the cell and probably formed a liquid layer. Such phenomenon has been already observed and discussed in a previous article dealing with the membrane formation using the PEI/NMP/water system.[27]

Comparison with numerical curves

The numerical model aimed at predicting the variation of the polymer composition during VIPS process. Thanks to the experimental measurements performed by NIRS at the three points of increasing depths in the solution, the model could be validated using experimental composition profiles. The experiments were performed for different process conditions (temperature and relative humidity), and different formulations (increasing polymer concentrations), hence, the comparison between the simulated results and the experimental data was first discussed for given operating conditions (40°C and 75% RH). Since both the Flory-Huggins theory and the

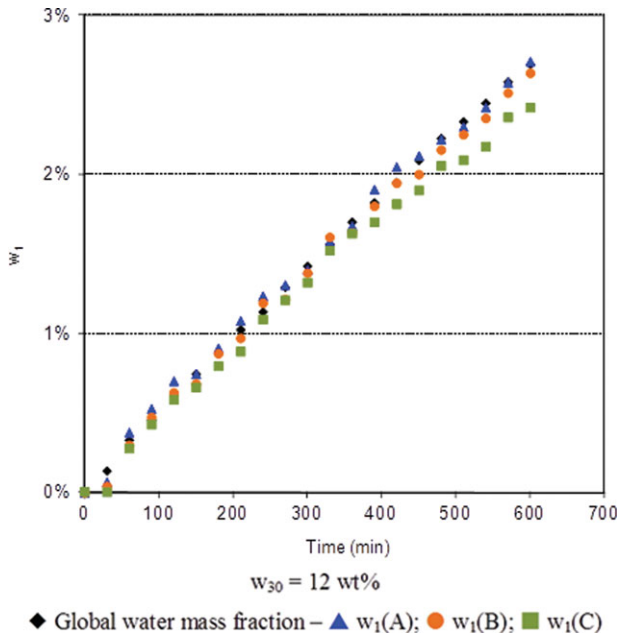

Figure 3. Variation as a function of time of the global water mass fraction and local water mass fractions at points A, B, and C: w_{30} = 12 wt. %, T = 25°C, and RH = 75%.

[Color figure can be viewed in the online issue, which is available at wileyonlinelibrary.com.]

diffusion formalism are only applicable in homogeneous polymer solutions, the simulated curves were plotted until the demixion time. Once the phase separation began, the model was no more relevant.

In the first part, the influence of the mass-transfer coefficient was discussed. For that, the following experimental conditions were chosen: polymer concentration in the initial solution equal to 12 wt. %, temperature and relative humidity in the fabrication chamber equal to 40°C and 75%, respectively. In the second part, the numerical results were compared with an experimental one for higher polymer concentrations and different operating conditions. In the third part, since the numerical model was shown to overestimate the diffusion kinetics within the solution at high-polymer concentration, the self-diffusion coefficient was discussed to improve the agreement between the numerical and experimental results.

Mass-transfer coefficient k_p. The numerical predictions obtained at 40°C and 75% RH for the lowest polymer concentration (12 wt. %) correspond to the simulation run S1 (the whole simulation conditions were summarized in Table 5). The simulated curves were plotted in Figure 4 and compared to experimental data.

Figure 4 exhibits that the agreement between the numerical predictions and the experimental data was fairly good; indeed, the model did not contain any adjustable parameter for this simulation run. Nevertheless, Figure 4 also exhibits that the model overestimated the mass-transfer rate during the first few minutes. The model predicted a rapid increase of the water concentration during 25 min and then a slope change occurred, leading to a slight reduction of the water intake rate. This trend was observed not only for the global water concentration but also for the local concentrations at points A, B, and C. This slope change could be explained in terms of external mass-transfer coefficients rather than internal diffusion since all kinetic curves were affected. To focus on this result, the variation of the mass-transfer coefficients for water (k_{p1}), and NMP (k_{p2}), as a function of time were plotted in Figure 5.

k_{p1} and k_{p2} directly depend on air motion above the solution due to free convection, which is controlled by a density change due to both temperature and concentration gradients. So, the variation of the temperature at the air/solution interface was also plotted. At the beginning of the VIPS process, the initial solution temperature was equal to the ambient temperature (20°C), and the initial water concentration in the solution was null. Therefore, heat- and mass-transfer rates were maximal during this initial period, because the driving force for each transfer was maximal also. Heat exchanges between the air and the polymer solution led to a temperature increase to reach a thermal equilibrium (the VIPS chamber temperature was equal to 40°C), and at the same time, the water concentration increased in liquid phase near the interface because of the water intake. Both effects led to a rapid reduction of the air density gradient in the vicinity of the air/solution interface, and, thus, to a rapid decrease of the external mass-transfer coefficients (Figure 5). k_{p1} and k_{p2} values were reduced by a factor 2.2 after only 25 min, and by a factor 3.2 after 40 min. Later during the process, the heat exchanges were reduced leading to lessening the free convection phenomena; consequently, the mass-transfer coefficients reached constant values until the end of the experiment.

Nevertheless, the rapid initial mass-transfer rates and the slope change obtained by the simulations were not in perfect agreement with the experimental data (Figure 4). These slight differences could be explained by geometry aspects: the cells used in the experiments were 10 × 10 mm^2 large and 30 mm in height. Since the solution thickness was only 18 mm in height, the air above the solution was trapped between the cell walls. The air motion may have been reduced despite density gradients. Since the simulated water and NMP mass-transfer coefficients reached a plateau after 1 h, these constant values were retained in the model for further simulations. The simulation run S2 was then performed; exhibiting that the agreement between the simulated and experimental curves was clearly improved (Figure 6).

Concentration Profiles. Concentration profiles simulated at 40°C under 75% RH and for a polymer concentration of 12 wt. % were plotted in Figure 7. They clearly exhibit the nonsolvent concentration gradients induced by the internal mass-transfer resistance, and proved that the phase separation progressed from the air/solution interface toward the bottom of the solution. Both solvent and polymer concentration profiles indicate the interface region (just beneath the air/solution interface) is a pseudolean polymer phase: the polymer concentration suddenly decreased in the vicinity of the interface, whereas the solvent concentration increased. Such simulated results were in agreement with the results

Table 4. Demixion Time for each Condition of Process and Formulation Condition

Temperature	Relative humidity	12 wt% PEI	16 wt% PEI	20 wt% PEI	25 wt% PEI
40 °C	75% RH	340	240	180	120
	43% RH	-	360	300	160

Table 5. Parameters used for the Simulations

Case	w_{10}	w_{20}	w_{30}	T	RH	Air flow conditions (NC: natural convection)	Average hole free volume
S1	10^{-7}	88 wt%	12 wt%	40 °C	75%	NC – variable mass transfer coefficients	$\frac{\hat{V}_{FH}}{\gamma}$
S2	10^{-7}	88 wt%	12 wt%	40 °C	75%	NC – constant mass transfer coefficients	$\frac{\hat{V}_{FH}}{\gamma}$
S3	10^{-7}	84 wt%	16 wt%	40 °C	75%	NC – constant mass transfer coefficients	$\frac{\hat{V}_{FH}}{\gamma}$
S4		80 wt%	20 wt%				
S5	10^{-7}	88 wt%	12 wt%	25 °C	75%	NC – variable mass transfer coefficients	$\frac{\hat{V}_{FH}}{\gamma}$
S6	10^{-7}	88 wt%	12 wt%	40 °C	43%	NC – constant mass transfer coefficients	$\frac{\hat{V}_{FH}}{\gamma}$
S7		84 wt%	16 wt%				
S8		80 wt%	20 wt%				
S9	10^{-7}	84 wt%	16 wt%	40 °C	75%	NC – constant mass transfer coefficients	$\frac{V_{FH}}{\gamma} \times \frac{0.25}{0.25 + w_1^{0.3}}$
S10		80 wt%	20 wt%				$\frac{V_{FH}}{\gamma} \times \frac{0.25}{0.25 + w_1^{0.25}}$
S11	10^{-7}	84 wt%	16 wt%	40 °C	43%	NC – constant mass transfer coefficients	$\frac{V_{FH}}{\gamma} \times \frac{0.25}{0.25 + w_1^{0.3}}$
S12		80 wt%	20 wt%				$\frac{V_{FH}}{\gamma} \times \frac{0.25}{0.25 + w_1^{0.25}}$

obtained by Khare et al.[11] who obtained the same kind of profiles with a similar system (PEI/PVP/NMP/water). The polymer concentration profiles simulated by the model were almost plate, characterized by low gradients in the solution depth, excepted in the vicinity of the interface. Such plate profiles could be explained by the low volatility of the solvent (NMP): the mass-transfer resistance in gas phase is very high due to low volatility; hence, the solvent extraction rate during the VIPS process is particularly low. The use of a volatile solvent such as acetone would strongly modify such polymer concentration profiles due to high-evaporation rate.[12,26] Even if all curves corresponding to other operating conditions were not plotted, the numerical model exhibited that the higher the polymer concentration, the higher the concentration gradients. Indeed, increasing the polymer concentration induced a reduction of the free volumes between the polymer chains, and, thus, a reduction of the diffusion rate. For a given process parameter, the internal mass-transfer resistance was enhanced for higher polymer concentration, whereas the external resistance did not change; therefore, the concentration gradients were enhanced.

Influence of the polymer concentration in the initial solution. The numerical predictions and experimental results were then compared for higher polymer concentrations at 40°C under 75% RH in simulation run S3 and S4 (Table 5), and the predicted curves were reported in Figure 8. For the simulation run, water and NMP mass-transfer coefficients k_{p1} and k_{p2} were kept constant since preliminary simulations had exhibited that their value was independent of the polymer concentration. Therefore, all further simulations performed at 40°C integrated the predicted mass-transfer coefficients at the plateau. The comparison between the simulated and experimental kinetic curves pointed out that the model overestimated the nonsolvent diffusion rate within the solution when the polymer concentration exceeded 12 wt. %. For a polymer concentration equal to 16 wt. %, the agreement between both curves was good during 100 min, but the slope change observed on experimental curves was not predicted by the numerical model. Moreover, the higher the polymer concentration, the higher the gap between simulated and experimental curves. For a polymer concentration equal to 20 wt. %, the gap between predicted and experimental curves was even more pronounced: a time lag was experimentally observed before the water detection at point A, whereas the simulated curves began increasing right from the VIPS process started. In this case (S4), the experimental kinetic curves obtained at points B and C (11 and 15 mm beneath the air/solution interface) exhibited a sudden slope change after 120 min, whereas the simulated curves kept on increasing without any slope change until the phase separation occurred.

Influence of the process parameters. Simulations were then tested (1) at a lower temperature (25°C), and (2) under a lower relative humidity (43=). The objective was to verify

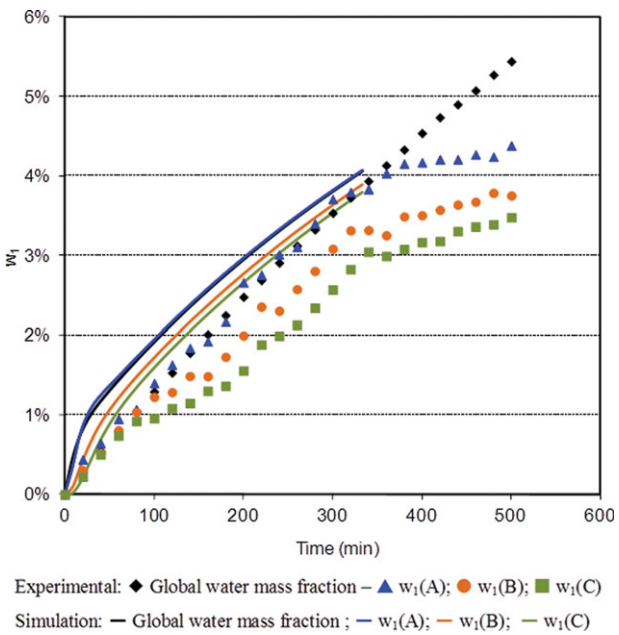

Figure 4. Simulation S1.

Comparison between numerical predictions and experimental data for w_{30} = 12 wt. %, T = 40°C, and RH = 75%. [Color figure can be viewed in the online issue, which is available at wileyonlinelibrary.com.]

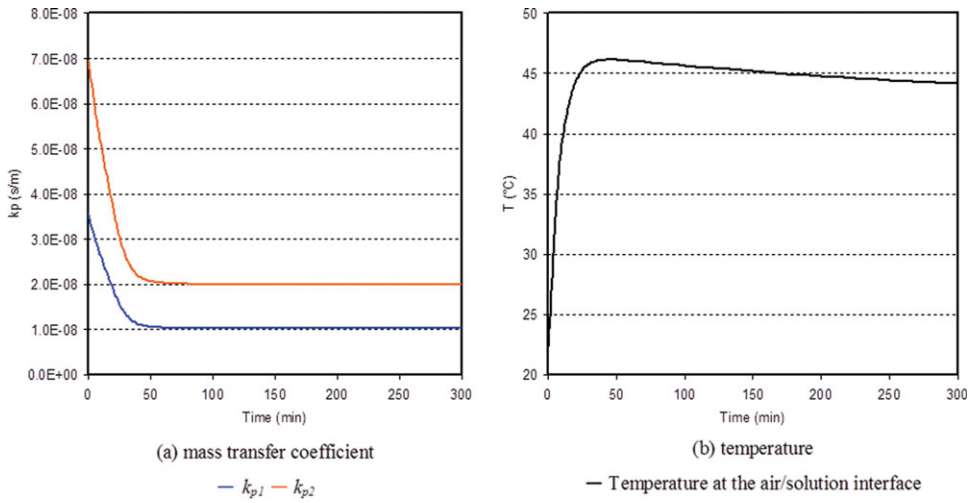

Figure 5. Simulation S1.

Variation of the mass-transfer coefficients and interface temperature during the process. Numerical predictions: w_{30} = 12 wt. %, T = 40°C, and RH = 75%. [Color figure can be viewed in the online issue, which is available at wileyonlinelibrary.com.]

whether the differences between experimental data and numerical predictions were similar to those observed at 40°C under 75% RH.

First, Figure 9, which reports the curves obtained for the simulation S5 performed at 25°C under 75% RH, confirmed the good agreement obtained at 12 wt. % of the polymer for various conditions of temperature. Besides, the temperature is the most interesting operating parameters for validating the model since a temperature modification affects the whole phenomena involved in the mass-transfer process: (1) The external mass-transfer coefficients depend on temperature, especially since free convection result from air density gradient in the vicinity of the interface: the air density is directly affected by a temperature change, hence, the Grashoff number and the mass-transfer coefficients too; (2) the temperature affects the external driving force for mass transfer; indeed, the solvent and nonsolvent concentrations at the air/solution interface depend on the local temperature; moreover, the temperature affects the nonsolvent concentration in gas phase (Eq. 9), and (3) the internal diffusion coefficients significantly depend on temperature in liquid phase as well (Eqs. 14, 15 and 16). So, a temperature change during the VIPS process affects not only the external mass-transfer resistance, but also the internal one. Consequently, the agreement between the numerical predictions and the experimental data obtained at two different temperatures is a strong and reliable validation of the mass-transfer model, for moderate polymer concentration. Moreover, in this case, the VIPS process was conducted at a temperature (25°C) close to the initial solution temperature (20°C), therefore, the temperature gradients were lower during the first minutes of the experiments, until the whole solution reached the chamber temperature; hence it was not necessary to fix the external mass-transfer coefficients and variable mass-transfer coefficients were integrated in the model.

The numerical predictions obtained under a lower relative humidity at the same polymer concentration (S6) also gave good results (Figure 10a). In this case, only the external mass-transfer resistance was affected by a decrease of RH. As a result, the numerical model gave reliable results whatever the process conditions once the polymer concentration was moderate (12 wt. %).

For higher polymer concentration (16 wt. %), the numerical model gave reliable predictions during 100 min, and then the experimental curves exhibited a slight slope change when the water concentration within the polymer solution almost reached 1 wt. %. At 20 wt. % of polymer, a short-time lag appeared before water was detected in the solution, whereas the model predicted immediate increase of the water concentration, thus, overestimating the nonsolvent-transfer rate. As for the simulation run performed under 75% RH,

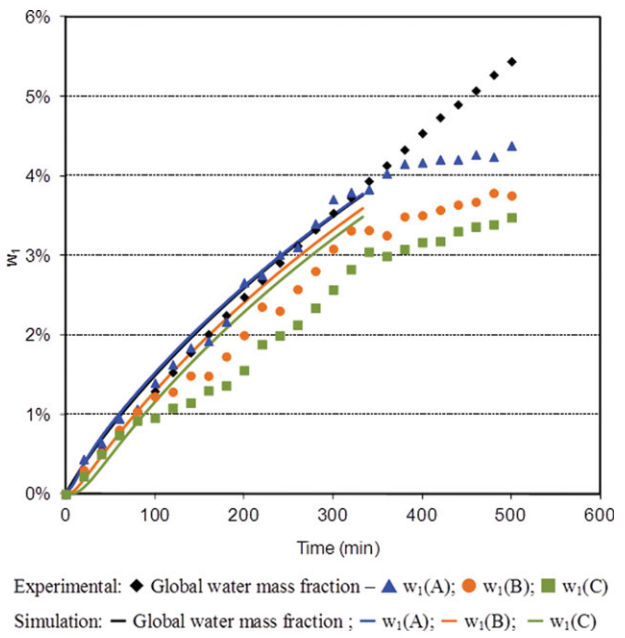

Figure 6. Simulation S2.

Comparison between numerical predictions and experimental data for w_{30} = 12, 16, and 20 wt. %, T = 40°C, and RH = 75%. $kp_1 = 1.0\ 10^{-8}$ s/m, and $kp_2 = 2.0\ 10^{-8}$ s/m. [Color figure can be viewed in the online issue, which is available at wileyonlinelibrary.com.]

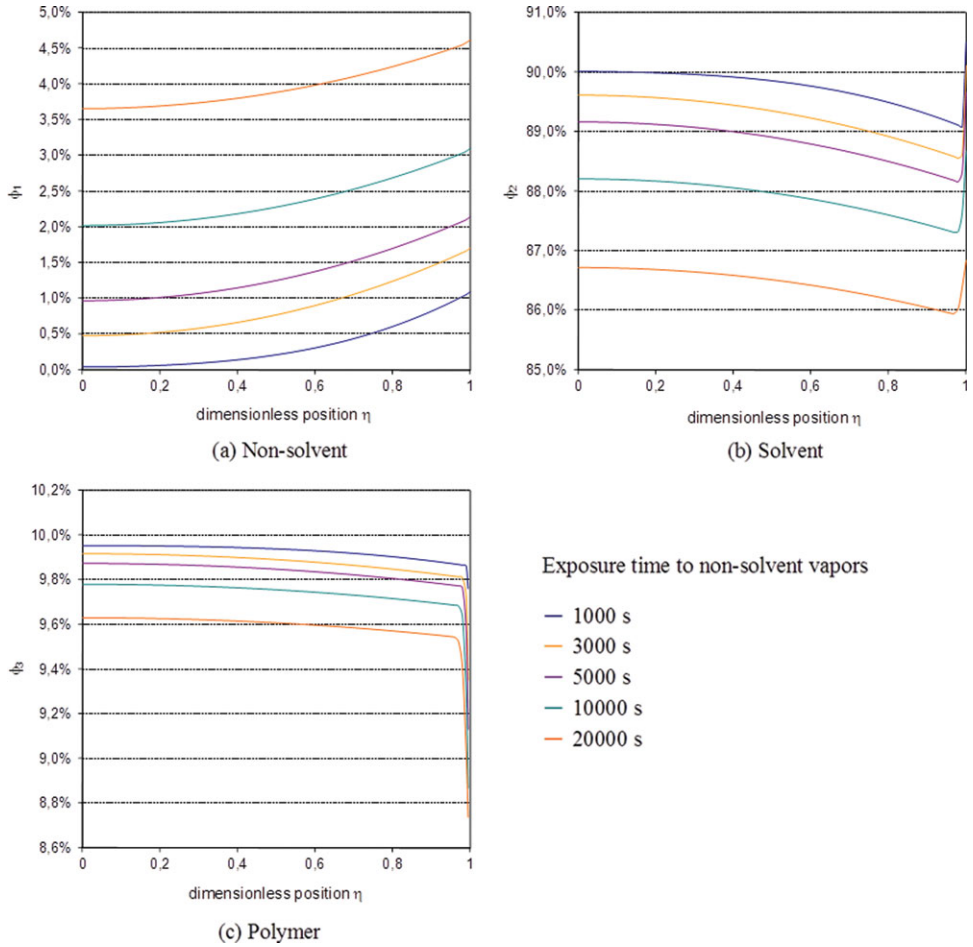

Figure 7. Concentration profiles of (a) nonsolvent, (b) solvent, and (c) polymer: w_{30} = 12 wt. %, T = 40°C and RH = 75%.

$kp_1 = 1.0\ 10^{-8}$ s/m, and $kp_2 = 2.0\ 10^{-8}$ s/m. [Color figure can be viewed in the online issue, which is available at wileyonlinelibrary.com.]

the gap between the numerical predictions and the experimental data increased when increasing the polymer concentration. In addition, the experiments conducted at 16 wt. % of polymer indicated that the decrease of nonsolvent rate was also linked to the amount of water within the solution. Such results, combined with the fact that at 12 wt. % of

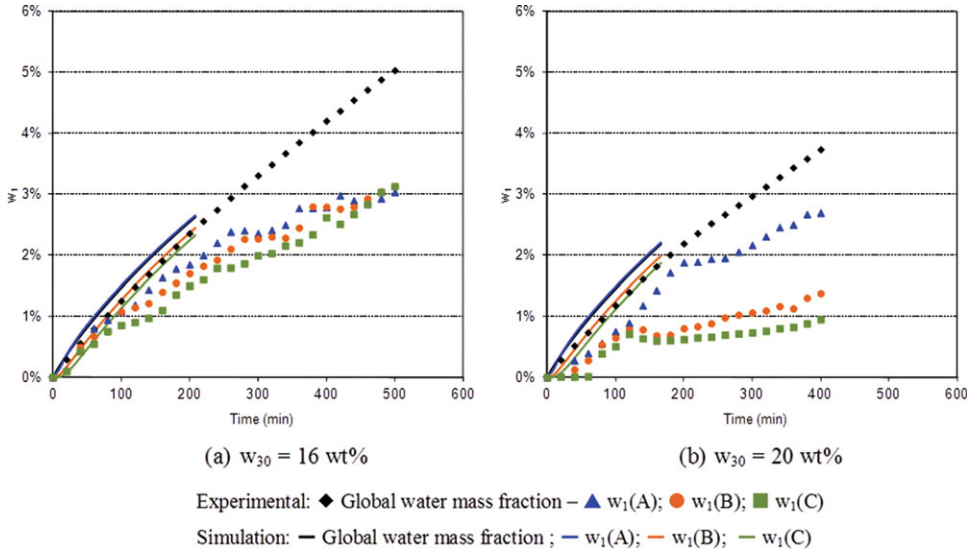

Figure 8. Simulation S3 and S4.

Comparison between numerical predictions and experimental data for w_{30} = 16 and 20 wt. %, T = 40°C, and RH = 75%. $kp_1 = 1.0\ 10^{-8}$ s/m, and $kp_2 = 2.0\ 10^{-8}$ s/m. [Color figure can be viewed in the online issue, which is available at wileyonlinelibrary.com.]

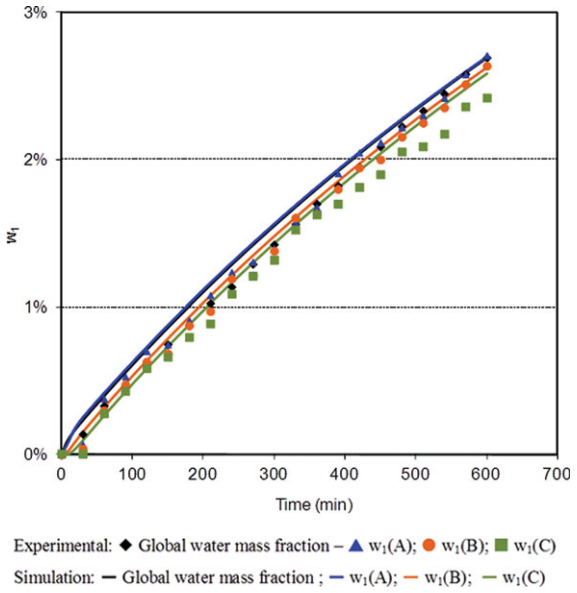

Figure 9. Simulation S5.

Comparison between numerical predictions and experimental data for w_{30} = 12 wt %, T = 25°C, and RH = 75%. Use of variable transfer coefficients. [Color figure can be viewed in the online issue, which is available at wileyonlinelibrary.com.]

polymer the model gave reliable predictions whatever the process conditions, pointed out that the model overestimated diffusion rate when the polymer concentration exceeded 12 wt. %.

Influence of the Water Concentration on PEI Solution Properties. These results exhibited that the model overestimated the diffusion rate for high-polymer concentrations, especially for high-nonsolvent concentration within the solution. Such phenomenon can be linked to a change in the polymer chain conformation in the polymer solution consecutively to the water penetration. Intramolecular interactions and intermolecular association could affect the mass-transport properties of small molecules through the polymer chains network by reducing the free volumes. The viscosity behavior of the PEI/NMP/water system has been investigated by Ripoche et al.[28] who focused on the influence of the nonsolvent concentration on the solution viscosity in concentrated polymer solutions. They have shown that the viscosity of the polymer system could be significantly modified by the water concentration, for different polymer concentrations in the range of 15–25 wt. % (Figure 11). For a polymer concentration of 15 wt. %, the viscosity gradually increased until the water concentration reached 2.5 wt. % and then suddenly dropped. For a polymer concentration of 25 wt. %, a drastic increase was observed once the water concentration only reached 1.5 wt. %. Thus, for concentrated polymer

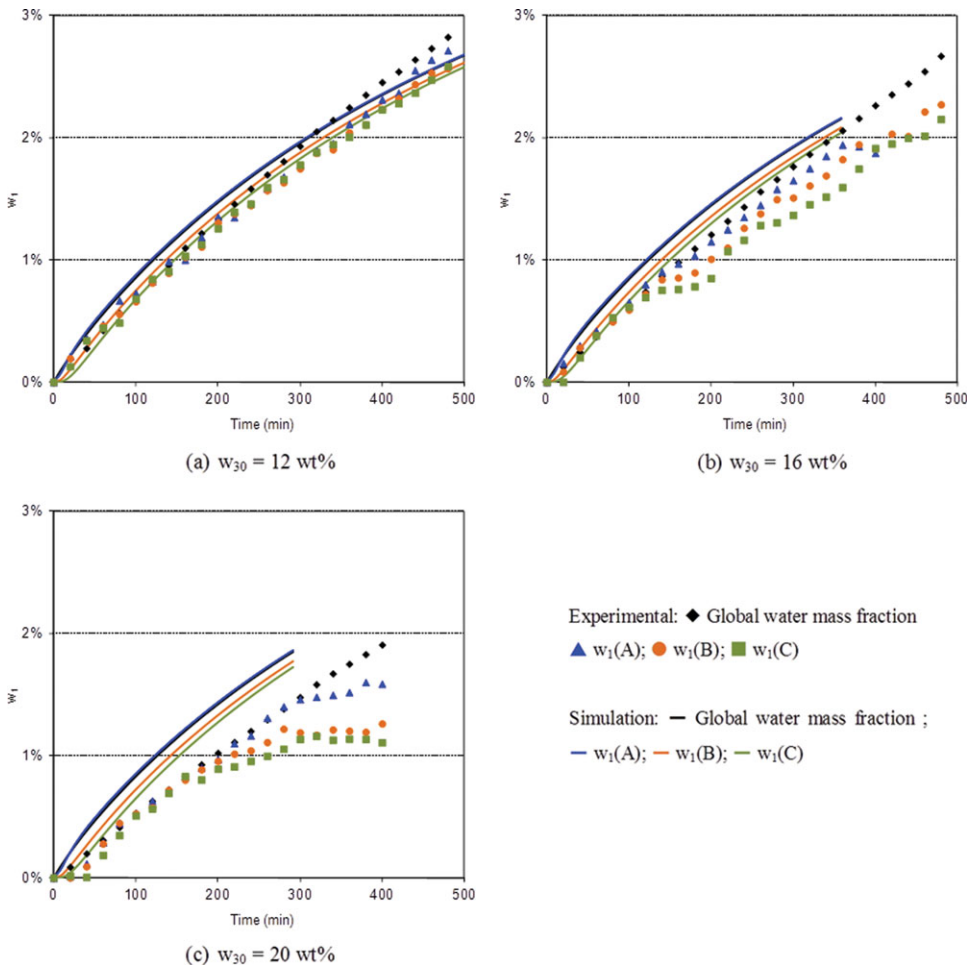

Figure 10. Simulation S6 to S8.

Comparison between numerical predictions and experimental data for w_{30} = 12, 16 and 20 wt. %, T = 40°C, RH = 43%. kp1 = 1.3 10^{-8} s/m, and kp2 = 2.2 10^{-8} s/m. [Color figure can be viewed in the online issue, which is available at wileyonlinelibrary.com.]

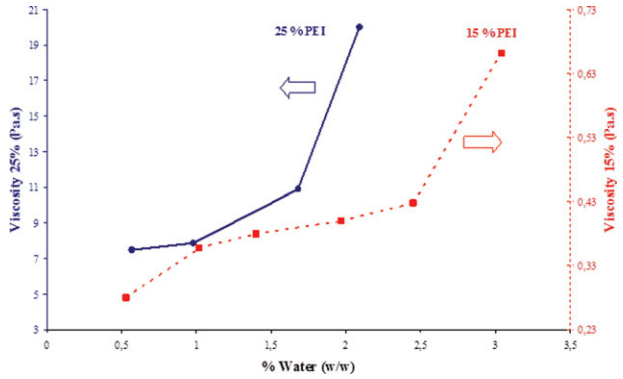

Figure 11. Viscosity at 40°C ternary solutions vs. the water content.[47]

[Color figure can be viewed in the online issue, which is available at wileyonlinelibrary.com.]

solutions, higher the PEI concentration, lower the water concentration to induce a viscosity increase and so to reinforce interactions between molecular chains leading to a reduction in chain mobility.

The viscometric behavior of the poly(ether imide) in binary mixtures NMP/water has been reported by Viallat et al.[29] in semidilute polymer solutions (0–8 wt. %). Results displayed an increase in viscosity at a given polymer concentration when water was added to NMP. These observations are in accordance with those given by Ripoche et al.[28] for higher PEI concentrations. Moreover, considerations on the intrinsic viscosity reported by Viallat et al.[29] have clearly demonstrated the influence of water on the state of the polymer solution. The intrinsic viscosity was found to decrease with increasing water content in NMP. This behavior was related to more compact macromolecular coils when water is present in NMP solution. The influence of water on chain contraction was not only associated with the reduction of the solvent quality consecutively to water addition, but was also attributed to specific interactions between water molecules and monomeric units of PEI. First, the formation of intramolecular and intermolecular charge-transfer complexes (CTC) in PEI solutions between electron donor (aromatic rings) and electron-acceptor groups (C=O groups) were evidenced by fluorescence spectroscopy[30] and may occur during our experiments. However, this aggregation process was found to be very slow in the absence of water.[30] CTC formation obeys a thermodynamic equilibrium which needs time to be reached. The creation of an intermolecular CTC complex requires that an electron-donor unit encounters an electron-acceptor unit of another chain with a favorable geometry. At high-polymer concentration (16 and 20 wt. % in this study) such interactions should be favored and, consequently, should have occurred more rapidly. Second, Viallat et al.[29] proposed also that water can form water-monomer CTC through associations by hydrogen bonds between one or two hydrogen atoms of a water molecule, with one or two carbonyl groups of the monomeric PEI unit into an intramolecular aggregate structure. In that case, increasing water content in ternary system may enhance the formation of water-monomer CTC.

Thus, we assumed that the formation of such inter- and intramolecular interactions in PEI solutions with time due to water penetration (aggregation process), should be responsible of a reduction of the free volumes by decreasing the chain mobility.

In this respect, since the model gave good predictions for 12 wt. % of PEI, the number of CTC established in the polymer solution is supposed not to be high enough to modify the water diffusion rate during the VIPS process for moderate polymer concentration. On the contrary, for higher polymer concentrations, the model overestimated the nonsolvent intake rate. This result was, thus, explained by a nonnegligible influence of the aggregation process on the polymer chain conformation occurring before the end of the experiments. Indeed, a slope change was experimentally observed when the water concentration reached a critical value, which depended on the polymer concentration. The agreement between both results confirmed that the solution properties were modified by water intake, inducing a decrease of the diffusion rate of nonsolvent, which moved from expanded polymer chains to chain contraction. It should be noted that

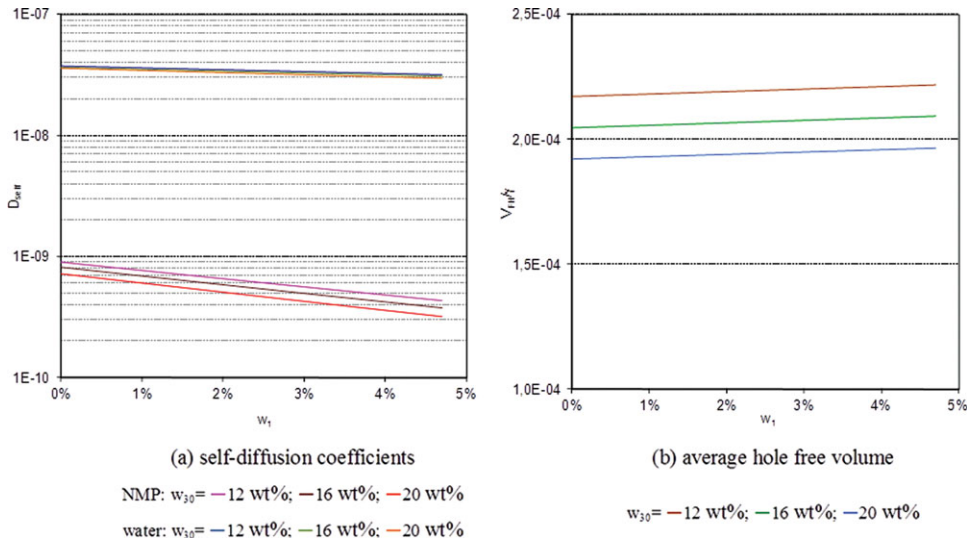

Figure 12. Influence of the polymer concentration and the water content on (a) the water and NMP self-diffusion coefficients, and (b) the average hole-free volume.

[Color figure can be viewed in the online issue, which is available at wileyonlinelibrary.com.]

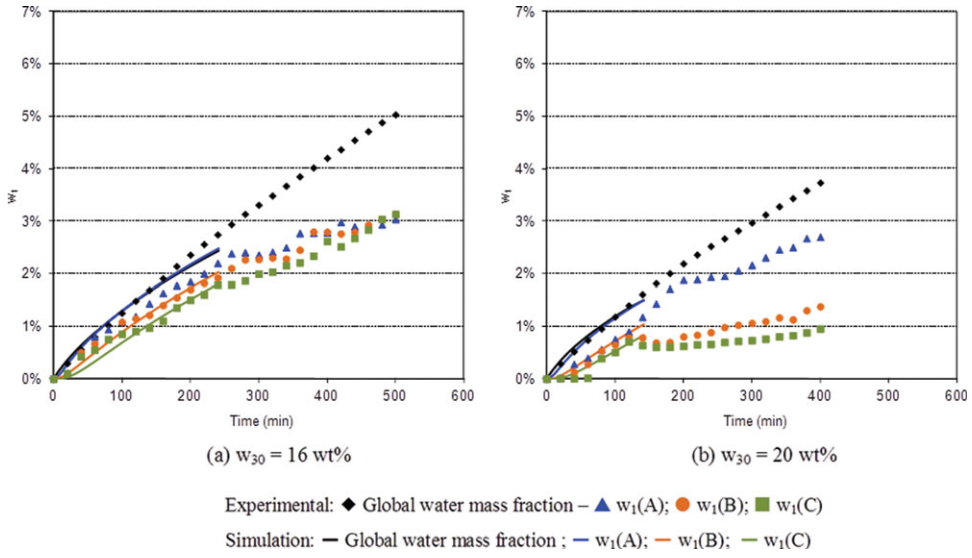

Figure 13. Simulation S9 and S10.

Comparison between numerical predictions and experimental data for w_{30} = 16 and 20 wt. %, T = 40°C, and RH = 75%. kp_1 = 1.0 10^{-8} s/m, and kp_2 = 2.0 10^{-8} s/m. [Color figure can be viewed in the online issue, which is available at wileyonlinelibrary.com.]

these phenomena occurred before demixion of the polymer solution. Chain aggregation in PEI solution was enhanced by water penetration until the solution phase-separated into two phases: a polymer rich-phase and a polymer lean-phase.

Modification of the self-diffusion coefficient. Unlike experimental data, the numerical model based on the Vrentas and Duda free-volume theory predicted a weak influence of both the polymer concentration and water content on the water intake rate, at least for the operating conditions presented in this article. So, the expressions of the self-diffusion coefficients should be discussed for improving the agreement between simulated and experimental results.

In the model, the diffusion equations are expressed in terms of cross-diffusion terms involving (1) the gradients of the chemical potential of each component, and (2) the self-diffusion coefficients expressed using the free-volume theory. Both water and NMP self-diffusion coefficients (Eqs. 14 and 15) involve 12 independent parameters whose values were found in the literature, including the average hole-free volume (V_{FH}/γ). Nevertheless, plotting the variation of non-solvent and solvent self-diffusion coefficients (D_{1self}-and D_{2self}, respectively) vs. the water concentration for increasing polymer concentrations exhibited that the nonsolvent concentration did not strongly affect both self-diffusion coefficients (Figure 12). D_{1self} and D_{2self} exhibited a decreasing trend when increasing both polymer concentration and water content; moreover, since water molecules are smaller than NMP molecules, the value of D_{1self} was less affected than

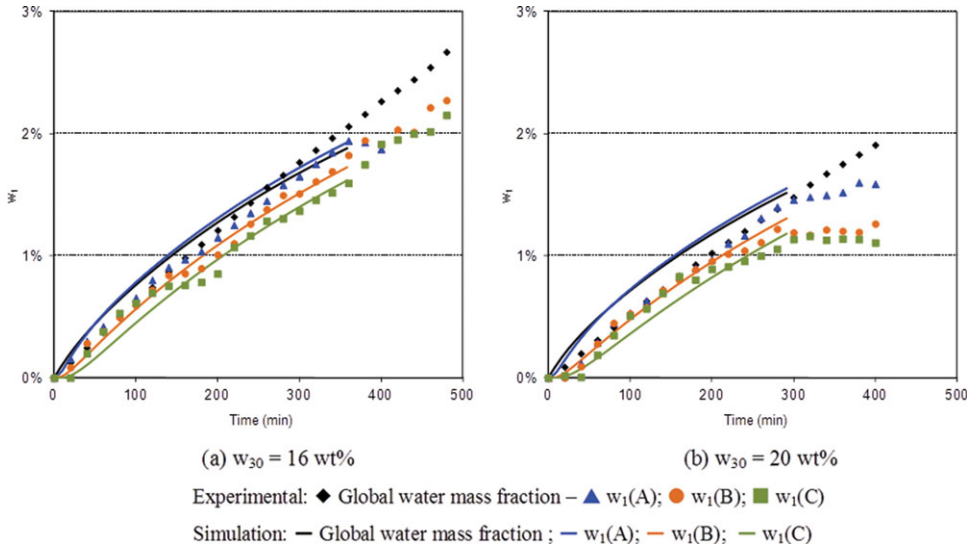

Figure 14. Simulation S11 and S12.

Comparison between numerical predictions and experimental data for w_{30} = 16 and 20 wt. %, T = 40°C and RH = 43%. kp_1 = 1.3 10^{-8} s/m, and kp_2 = 2.2 10^{-8} s/m. [Color figure can be viewed in the online issue, which is available at wileyonlinelibrary.com.]

D_{2self} when increasing both nonsolvent and polymer concentrations. The variation of the hole-free volume was reported in the same figure, and exhibited similar trend: increasing the polymer concentration induced a reduction of the average free volume, but the water concentration was shown to slightly affect its value. So, even if the model predicted a decrease of the nonsolvent intake rate in polymer matrix when increasing both polymer and nonsolvent concentrations, the magnitude of the decrease was clearly underestimated since diffusion coefficients were weakly affected. The strong modification of the polymer matrix observed by viscosity measurements (in agreement with *in situ* mass-transfer analysis performed by NIRS) was not taken into account in the diffusion model, but it was shown to strongly affect the mass-transfer rate.

In this context, it was interesting to investigate which parameter(s) included in the self-diffusion expression could be affected by the water concentration, especially for high-polymer concentrations. D_0 is the pre-exponential factor; its value is constant and is not expected to depend on polymer solution properties. V_i^* is the specific critical hole-free volume of component i required for a jump. Since those parameters are associated with the intrinsic transport ability of component i, they were not expected to depend on solution composition. The average hole-free volume (V_{PH}/γ) integrates three volume parameters associated with the polymer ($K_{13}/K_{23} - T_{g3}$), the solvent (K_{12}/γ, $K_{22} - T_2$), and the nonsolvent (K_{11}/γ, $K_{21} - Tg_1$). Six parameters being involved in the hole-free volume expression, it was tricky to correlate them separately to the macromolecular interactions induced by water intake. Therefore, it was chosen to multiply the average hole-free volume by a factor taking into account the influence of both the polymer and the water concentration. This multiplicative factor was used for polymer concentration higher than 12 wt. %. It contains two parameters, which have to be determined by fitting the numerical predictions and the experimental data, and it indicates that the average hole-free volumes were expected to decrease with increasing the water concentration, especially for high-polymer concentrations

$$\frac{V_{FH}}{\gamma}_{m} = \frac{V_{FH}}{\gamma} \times \frac{x}{x + w_1^{y(w_{3i})}} \tag{16}$$

The multiplicative factor was equal to unity for null water concentration, i.e., for binary solvent/polymer solutions. The value of y increased while increasing the polymer concentration in the initial solution.

The simulation results including the modified expression of the average hole-free volume were first performed at 40°C under 75% RH, for polymer concentrations higher than 12 wt. %, i.e., 16 and 20 wt. %. These simulation runs correspond to S9 and S10 (Figure 13), and the resulting curves were reported in Figure 13. The better agreement between numerical and experimental data confirmed that the mass-transport phenomena within the polymer matrix were better simulated after modification of the hole-free volume expression. The parameters used in the modified model were slightly different depending on the polymer concentration since the influence of nonsolvent content was shown to depend on the polymer concentration. Those results obtained at 40°C under 75% RH were promising, but they had to be confirmed using other operating conditions.

So, the simulations S11 and S12 were performed at the same temperature under 43% RH (Table 5). For these simulations, the modified expressions of the hole-free volume (V_{FH}/γ) were the same as those used for simulations S9 and S10, which corresponded to polymer concentrations equal to 16 and 20 wt. %, respectively. In this respect, the parameters used in the modified self-diffusion expressions depended only on the polymer concentration, but not on the other operating parameters. Figure 14 exhibits that the modified expression of V_{FH}/γ still gave good predictions when conducting the VIPS process under lower relative humidity, i.e., reducing the driving force for nonsolvent transfer. The agreement between experimental data and numerical predictions were not perfect at the three points of measurements, meaning that the diffusion phenomena in such a complex polymer matrix, whose properties may change during the VIPS process because of water intake, are very complex and tricky to simulate. Nevertheless, it was chosen not to add fitting parameters for artificially improving the agreement between experimental and numerical results; indeed, the use of too many fitting parameters should lessen the interest and the scope of the model for understanding the mass-transfer mechanisms involved in VIPS process. Moreover, the model applicability to various operating conditions would be reduced if too many parameters would be added to reach a perfect fit with the experimental data whatever the operating conditions.

Conclusion

This work presented a comparison between experimental kinetic data and the corresponding simulation results during the VIPS process for the ternary PEI/NMP/water system. The experimental data was collected in a rectangular cell where all the process parameters were controlled (T, HR and air flow). The VIPS process was conducted at two different temperatures (25 and 40°C) under two conditions of relative humidity (43 and 75%); airflow was controlled by free convection above the air/solution interface, and increasing polymer concentrations in the initial solution were tested (12, 16, and 20 wt. %). The nonsolvent intake rate in the polymer solution was followed by *in situ* NIRS measurements at three points at increasing depth from the air/solution interface and by gravimetric measurements. The numerical model involves the Flory-Huggins theory, cross-diffusion formalism, and the free-volume theory developed by Vrentas and Duda for the self-diffusion coefficients. This article proposed the first local validation of such mass-transfer model using *in situ* composition measurements. The comparison between experimental data and numerical predictions exhibited that the model accurately simulated the nonsolvent intake rate for a moderate polymer concentration (12 wt. %) in various conditions of temperature and relative humidity. For higher polymer concentration (16 and 20 wt. %), the model was shown to overestimate the nonsolvent diffusion rate. This result was explained in terms of polymer–polymer interactions and polymer-water interactions due to nonsolvent intake related to the establishment of charge-transfer complexes in PEI solutions. Indeed, these interactions at a molecular scale leading to

polymer aggregation were expected to strongly affect the mass-transfer mechanisms by modifying the free volumes within the polymer matrix. A modified expression of the average hole-free volume was proposed in this work to take into account the influence of the nonsolvent intake on diffusion phenomena; given a polymer system, the parameters used in the modified model only depended on the polymer concentration. Using the modified model for various RH conditions, the agreement between the numerical predictions and the experimental data were significantly improved, whatever the external mass-transfer resistance. These results indicated that the average hole-free volume was the relevant parameter to adjust for taking into account the modification of the transport ability due to nonsolvent intake in the polymer solution.

Notation

a_i = activity of component i
D_{ig} = diffusion coefficient of component i in the gaseous phase, m^2/s
D_{0i} = pre-exponential factor of component i, m^2/s
g = gravitational acceleration, g m/s^2
g_{12} = solvent/nonsolvent interaction parameter
Gr = Grashof number
h = heat-transfer coefficient above the solution, $J/m^2.s.K$
H = polymer solution thickness, m
J_i^g = flux of i in the gas phase, $kg/m^2.s$
k_i = mass-transfer coefficient, m/s
k_{pi} = mass-transfer coefficient, s/m
K_{1i}/γ = free-volume parameter of component i, $m^3/(kg.K)$
$K_{2i} - T_{gi}$ = free-volume parameter of component i, K
Lc = characteristic length of the system, m
M_i = molar mass of component i, kg/mol
$M_{i,\mathrm{air}}$ = kg/mol
M_{air} = molar mass of air, kg/mol
n_i = number of mole of component i, mole
P = total pressure in the gas phase, Pa
P_i^0 = saturated pressure of NMP and water, Pa
Pr = Prandtl number
R = ideal gas constant, J/K.mol
Sc = Schmidt number
T = temperature of the solution, K
T_0 = initial temperature of the solution (ambient temperature), K
T^i = temperature at the air/solution interface, K
T^g = temperature in the gas phase, K
Σv = diffusion volume, m^3
$\hat{V}_i$ = partial specific volume of component i, m^3/kg
$\hat{V}_{ig}$ = partial specific volume of component i in the gaseous phase, m^3/kg
$y_{\mathrm{air,lm}}$ = Log mean mole difference of air

Greek letters

ρ_i = concentration of component i in the polymer solution, kg/m^3
ρ_{ig}^i = concentration of component i at the air/solution interface in the gas phase, kg/m^3
ρ_{ig}^∞ = concentration of component i in the bulk in the gas phase, kg/m^3
ρ_{air} = density of the air, kg/m^3
ρ_p = density of the solution, kg/m^3
ϕ = volume fraction
μ_i = chemical potential of component i, J/mol
ΔG_m = Gibbs free-energy-of-mixing
β = coefficient of volumetric thermal expansion, 1/K
χ_{13} = polymer/nonsolvent interaction parameter
χ_{23} = polymer/solvent interaction parameter
ζ_{ij} = ratio of critical molar volume of jumping unit of component i to that of component j
λ_p = thermal conductivity of polymer solution, J/(s.m.K)
C_{p_p} = heat capacity of the polymer solution, J/(kg.K)
λ_g = thermal conductivity of the air
μ_{air} = dynamic viscosity of gaseous phase, Pa.s
ΔH_{vi} = J/kg vaporization enthalpy of component i, J/(s.m.K)

Literature Cited

1. Smolders CA, Reuvers AJ, Boom RM, Wienk IM. Microstructures in phase-inversion membranes. Part 1. Formation of macrovoids. *J Membr Sci*. 1992;73(2–3)259–275.
2. Stropnik Č, Germič L, Žerjal B. Morphology variety and formation mechanisms of polymeric membranes prepared by wet phase inversion. *J Appl Polym Sci*. 1996;61(10)1821–1830.
3. Kim YD, Kim JY, Lee HK, Kim SC. Formation of membranes by immersion precipitation. II Morphology formation. *J Appl Polym Sci*. 1999;61:2124–2132.
4. Lai J-Y, Lin F-C, Wu T-T, Wang D-M. On the formation of macrovoids in PMMA membranes. *J Membr Sci*. 1999;155(1)31–43.
5. Lin D-T, Cheng L-P, Kang Y-J, Chen L-W, Young T-H. Effects of precipitation conditions on the membrane morphology and permeation characteristics. *J Membr Sci*. 1998;140(2)185–194.
6. Matsuyama H, Teramoto M, Nakatani R, Maki T. Membrane formation via phase separation induced by penetration of nonsolvent from vapor phase. I. Phase diagram and mass transfer process. *J Appl Polym Sci*. 1999;74(1)159–170.
7. Chae Park H, Po Kim Y, Yong Kim H, Soo Kang Y. Membrane formation by water vapor induced phase inversion. *J Membr Sci*. 1999;156(2)169–178.
8. Caquineau H, Menut P, Deratani A, Dupuy C. Influence of the relative humidity on film formation by vapor induced phase separation. *Polym Eng Sci*. 2003;43:798–808.
9. Menut P, Pochat-Bohatier C, Deratani A, Dupuy C, Guilbert S. Structure formation of poly(ether-imide) films using nonsolvent vapor induced phase separation: relationship between mass transfer and relative humidity. *Desalination*. 2002;145(1–3)11–16.
10. Chinpa W, Bouyer D, Pochat-Bohatier C, Deratani A., Dupuy C. Effect of a drying pretreatment on morphology of porous poly(ether-imide) membrane prepared using vapor-induced phase separation. *Drying Technol*. 2006;24:1317–1326.
11. Khare VP, Greenberg AR, Krantz WB. Vapor-induced phase separation--effect of the humid air exposure step on membrane morphology: Part I. Insights from mathematical modeling. *J Membr Sci*. 2005;258(1–2)140–156.
12. Yip Y, McHugh AJ. Modeling and simulation of nonsolvent vapor-induced phase separation. *J Membr Sci*. 2006;271(1–2)163–176.
13. Alsoy S, Duda JL. Modeling of multicomponent drying polymer films. *AIChE J*. 1999;45(4)896–905.
14. Shojaie SS, Krantz WB, Greenberg AR. Dense polymer film and membrane formation via the dry-cast process part I. Model development. *J Membr Sci*. 1994;94(1)255–280.
15. Bearman RJ. On the molecular basis of some current theories of diffusion. *J Phys Chem*. 1961;65(11)1961–1968.
16. Bouyer D, Werapun W, Pochat-Bohatier C, Deratani A. Morphological properties of membranes fabricated by VIPS process using PEI/NMP/water system: SEM analysis and mass transfer modeling. *J Membr Sci*. 2010;349(1–2)97–112.
17. Caneba GT, Soong DS. Polymer membrane formation through the thermal-inversion process. 2. Mathematical-modeling of membrane-structure formation. *Macromolecules*. 1985;18:2545–2555.
18. Altinkaya SA, Yenal H, Ozbas B. Membrane formation by dry-cast process: Model validation through morphological studies. *J Membr Sci*. 2005;249(1–2)163–172.
19. Li D, Krantz WB, Greenberg AR, Sani RL. Membrane formation via thermally induced phase separation (TIPS): Model development and validation. *J Membr Sci*. 2006;279(1–2)50–60.
20. McHugh AJ, Miller DC. The dynamics of diffusion and gel growth during nonsolvent-induced phase inversion of poly(ether sulfone). *J Membr Sci*. 1995;105:121–136.
21. Barton BF, Reeve JL, McHugh AJ. Observations on the Dynamics of Nonsolvent-Induced Phase Inversion. *J Polym Sci Part B Polym Phys*. 1997;35:569–585.
22. Pochat-Bohatier C, Werapun W, Bouyer D, Chinpa W, Deratani A. Near-infrared spectroscopy for the quantitative determination of mass transfer and water absorption kinetics by a polymer solution. *J Polym Sci Part B Polym Phys*. 2010;48:1960–1969.
23. Vrentas JS, Duda JL. Diffusion in polymer systems - 1. Reexamination of the free-volume theory. *J Polym Sci Polym Phys Ed*. 1977;15(3)403–416.

24. Vrentas JS, Duda JL, Ling H-C. Self-diffusion in polymer-solvent-solvent systems. *J Polym Sci Part A Polym Phys.* 1984;22(3)459–469.
25. Wei Y-M, Xu Z-L, Yang X-T, Liu H-L. Mathematical calculation of binodal curves of a polymer/solvent/nonsolvent system in the phase inversion process. *Desalination.* 2006;192(1–3)91–104.
26. Altinkaya SA, Ozbas B. Modeling of asymmetric membrane formation by dry-casting method. *J Membr Sci.* 2004;230(1–2)71–89.
27. Menut P, Su YS, Chinpa W, Pochat-Bohatier C, Deratani A, Wang DM, Huguet P, Kuo CY, Lai JY, Dupuy C. A top surface liquid layer during membrane formation using vapor-induced phase separation (VIPS)-evidence and mechanism of formation. *J Membr Sci.* 2008;310(1–2)278–288.
28. Ripoche A, Menut P, Dupuy C, Caquineau H, Deratani A. Poly (ether imide) membrane formation by water vapour induced phase separation. *Macromol Symp.* 2002;188:37–48.
29. Viallat A, Pedro Bom R, Cohen-Addad JP, Perez S. Viscosity behaviour of poly(ether imide) in solution: intramolecular interaction and intermolecular association effects. *Polymer.* 1992;33(20)4379–4383.
30. Viallat A, Pedro Bom R, Cohen-Addad JP, Charge-transfer interaction and chain association in poly(ether imide) solutions: a fluorescence spectroscopic study. *Polymer.* 1994;35(13)2730–2736.

Manuscript received Oct. 25, 2011, and revision received Apr. 2, 2012.